Evolution of Ferroelectric Domain Structures Embedded Inside Polycrystalline $BaTiO_3$ during Heating

Mesut Varlioglu,[1] Ersan Ustundag,[2,a] Nobumichi Tamura[b] and Jacob L. Jones[c]

[1]Iowa State University, Materials Science and Engineering, Ames, IA, 50011, USA,

[2]Advanced Light Source, Lawrence Berkeley National Laboratory, Berkeley, CA, 94720, USA

[3]University of Florida, Department of Materials Science and Engineering, Gainesville, FL, 32611, USA

Abstract

The evolution of ferroelectric domains inside a single grain of a polycrystalline $BaTiO_3$ ceramic was investigated under quasistatic heating by using polychromatic scanning X-ray microdiffraction (μSXRD). Four domain orientations were observed, three of which exhibited a classic ~90° ferroelastic relationship. The fourth domain orientation was found to be crystallographically related to one of the other orientations by a rotation of either 180.47° or 0.47°. While heating the polycrystalline $BaTiO_3$ from room temperature to above the Curie temperature (125°C), all four ferroelectric domain orientations rotated towards a paraelectric cubic orientation which was found to be at an intermediate orientation relative to the four domain orientations. The crystallographic relationships of the domains with respect to paraelectric phase were explained using a domain structure model by Nepochatenko.

Keywords: ferroelectricity, ceramics, X-ray microdiffraction, $BaTiO_3$, ferroelectric domains.

[a] Electronic mail: ustundag@iastate.edu

I. INTRODUCTION

Ferroelectric materials have been extensively used in microelectronic and sensing applications for more than 50 years because of their excellent piezoelectric properties[1]. $BaTiO_3$ was one of the first commercially viable ferroelectrics[2] and has been one of the most widely investigated ferroelectrics with its simple and well-known structure[3]. Upon cooling from a paraelectric phase, the polar axes of the individual unit cells within a ferroelectric $BaTiO_3$ can orient in certain crystallographic directions to minimize the overall energy of the system[4]. Clusters of these individual unit cells that are oriented in the same direction are called ferroelectric domains. The orientation of the domains depends on the crystal structure and the spontaneous polarization of the ferroelectric domains can be parallel to a cube edge (6 possible directions in total), body diagonal (8) and face diagonal (12) for tetragonal, rhombohedral and orthorhombic symmetries, respectively[5]. For tetragonal perovskite ferroelectrics, the final microstructure is composed of 90° and 180° domains where the polarization vectors of adjacent domains are perpendicular and parallel to each other, respectively. Since the c/a ratio of $BaTiO_3$ is not unity, γ, the angle between c axes of two 90° domains is

$$\gamma = 2\tan^{-1}\left(\frac{a}{c}\right) \quad (1)$$

For example, γ = 89.44° for polycrystalline $BaTiO_3$ with c/a=1.0098[6]. Therefore, the angle between *a* and *c* axes of two adjacent domains is 0.54°.

Due to the relative ease of conventional ceramic processing[7-8], the most commonly employed ferroelectrics are processed in polycrystalline form in which the material is composed of a collection of crystallographic grains with distinct orientations. In ferroelectric polycrystalline materials, each grain contains domains that are oriented with respect to one another by specific crystal symmetry operations. The domains belonging to the same grain are referred to as domain variants. The domain structure in ferroelectric ceramics exhibits a more complex pattern compared to single crystals. Several techniques such as transmission electron microscopy (TEM)[9-10], White Beam Topography[11], Electron Back

Scattering Diffraction[12], optical microscopy and atomic force microscopy[13-14], etc. have been used to characterize the ferroelectric domain structure but quantitative information on the orientation, strain and mesoscale dynamics within the ferroelectric domains are often lacking.

Temperature dictates both the formation of the ferroelectric phase from the paraelectric phase and the lattice aspect ratio of the ferroelectric phase, the latter of which affects the orientation relationships between domains (Eq. 1). Experiments as a function of temperature can therefore be useful to measure the evolution of mesoscale domain patterns in polycrystalline ferroelectrics. During cooling from an elevated temperature, the domain variants experience a phase transformation from cubic to tetragonal and the orientation of the grain can be distinctly determined.

Ferroelectrics are extremely sensitive to the nature of the surface, defect structure, sample preparation[15-16] and sample geometry[17]. Therefore, surface-sensitive characterization techniques may measure behavior that is not representative of the bulk. Synchrotron-based polychromatic Scanning X-Ray Microdiffraction (μSXRD), on the other hand, is a promising non-destructive tool with greater penetration depth than these other techniques (25μm penetration depth in $BaTiO_3$ at 5-16 keV as compared to 5 μm using conventional laboratory X-rays or electron microscopy), adequate resolution in strain (0.02%) and crystallite orientation (0.01°) as well as microfocusing capability providing submicron spatial resolution[18]. The fundamental principles of Laue or polychromatic X-Ray microdiffraction have been described elsewhere[19] and only a brief introduction is provided here. Laue microdiffraction utilizes microfocused polychromatic X-rays to illuminate an area of the sample as small as 1 μm^2. Multiple diffracting planes then provide a Laue diffraction pattern of individual crystalline grains from a small region of material embedded in a polycrystalline material. Laue microdiffraction can be used in scanning mode (polychromatic μSXRD) by raster-scanning the sample under the X-ray microbeam and measuring a Laue pattern at each step to obtain orientation and/or strain maps of the sample. Furthermore, the recent implementation of fast data acquisition and analysis programs such as XMAS (X-Ray Micro Analysis Software)[20] as well as the development of high-precision diffractometers[20] provides unique opportunities for μSXRD. In the present work, the μSXRD

technique is used to study the local, microscale and mesoscale behavior of polycrystalline ferroelectric materials during heating.

II. EXPERIMENTAL

A polycrystalline $BaTiO_3$ ceramic was prepared using conventional high temperature sintering[21] of $BaTiO_3$ powder (99.9% purity, with Ba/Ti ratio=1.00, Ferro Corp., Transelco Division). Figure 1 shows the SEM image of the $BaTiO_3$ sample investigated in this study. The nominal grain size was measured as approximately 20 μm as determined from an independent EBSD study with a $BaTiO_3$ sample from the same batch. The sample dimensions measured 1 mm x 1 mm x 5 mm and no electric field was applied prior to the experiment. The sample was attached on a heating element by using high temperature conductive glue (AA-Bond 200 Adhesive) to prevent sample movement during heating. The heating stage consists of a sample holder and a heating element bound by an Indium-Gallium coating to increase the conductivity. The temperature profile was monitored by one thermocouple attached to the surface of the sample (Fluke 87IV True RMS Thermometer), one from the heating element (Extech 421307 thermometer) and one with the IR thermometer (Extech Mini IR Thermometer 42500) pointed to the surface of the sample throughout the experiment. The sample was heated with steps up to and above the Curie temperature. The temperature variation between the thermometers did not exceed ±5°C for any temperature step.

For capacitance measurements, a sample was selected from the same batch and its surface was polished with fine paper to remove any surface contamination. The sample surfaces were sputtered with gold and a drop of silver paint was placed on the top of the electrodes to ensure a good electrical contact. Capacitance measurements were conducted using a Keithley 3330 LCZ meter at 0.1, 1, 10, and 100 kHz. Capacitance versus temperature measurements took place in an environmental chamber by heating up to 150°C with 5°C/min heating rate and cooling back to room temperature. The capacitance response of the $BaTiO_3$ sample was recorded during the heating followed by cooling and only the heating part is included the present work because the measurements during cooling are identical to

those measured during heating. The temperature was measured with a thermocouple placed in the vicinity of the sample.

μSXRD experiments were carried out on the X-ray microdiffraction end-station (7.3.3) at the Advanced Light Source (ALS). The instrument has a capability of delivering an X-ray white beam (5-14 keV) with less than 1 μm beam size by using a pair of elliptically bent mirrors in a Kirkpatrick-Baez configuration[19]. The diffraction patterns were collected with an area scan at room temperature and repeating at higher temperature steps. At each position of the area scans, the sample was exposed to X-rays for 2 seconds. The back-reflection Laue diffraction patterns produced by the white X-rays with 1 μm beam size were recorded using an X-ray CCD detector (MAR133) mounted on a vertical slide. The active area of the CCD camera had a diameter of 133 mm and the 1024 x 1024 pixels binned mode was used. The sample surface was set at 45° relative to the incoming beam and the detector. The distance from the CCD to the sample was determined to be 63.00 mm and the position of the center of the diffraction patterns on the CCD detector was determined to be at the pixel position (640.5,514.2).

The collected white-beam (Laue) diffraction patterns were analyzed with the custom XMAS software developed at the ALS. XMAS is capable of determining the positions of the reflections with subpixel resolution by using two-dimensional profile functions such as Gaussian, Lorentzian or Pearson VII. By using the peak positions and lattice parameters of $BaTiO_3$, each reflection was indexed with (hkl) indices. After indexing, the crystal orientations as an orientation matrix and the deviatoric strain tensor were obtained for each domain belonging to the illuminated area. The lattice parameter values of $BaTiO_3$ at room temperature used for the indexing procedure were a = 3.9947 Å and c = 4.0336 Å[8].

The orientation matrices in XMAS define the coordinates of the crystallites in the sample coordinate system unlike the standard definition of the orientation matrices as the direction cosines between the crystallites and the sample axes. Therefore, the orientation matrices must be normalized with the corresponding lattice parameters to convert the standard orientation matrices. The resultant orientations are a set of rotations that are a function of crystal symmetry. A proper representation of the

orientations is important because the misorientations between differing orientations should be independent of the crystal symmetry. Therefore, the orientations are required to be mapped to a unique solution, the so-called fundamental region[23] in the orientation space. The fundamental region[24] represents a region in the orientation space where the all symmetrically equivalent orientations can be mapped into a uniquely determined one. In order to find the misorientation between the orientations of the domains, the orientations were mapped into the corresponding fundamental region with the symmetry operators in corresponding crystal structures. The fundamental regions of the structure in the high temperature and low temperature regimes were determined using m3m and 4mm point symmetry respectively. The misorientations between the cubic-to-tetragonal and tetragonal-to-tetragonal orientations were calculated by using ODF/PF software package from Cornell University[22,25]. As the misorientation convention, angle-axis pairs were used. This convention has a major advantage to show the misorientation angle and axis with respect to a reference orientation, information that is helpful when describing the misorientation angle between domains.

III. RESULTS AND DISCUSSION

Fig. 2 shows the capacitance versus temperature profile of the $BaTiO_3$ sample measured at several different frequencies. The peak in capacitance was measured as 125.32 °C ± 0.06°C for all four frequencies.

Diffraction images were collected from the polycrystalline $BaTiO_3$ ceramic as a function of temperature. At a given fixed temperature, an area of the sample of size 50 µm x 50 µm was scanned using the 1 µm beam in steps of 1.5 µm. At room temperature, the diffraction pattern shows four close spots. One of these grains was selected as reference and the diameter of this grain was found to be 16.5 µm by translating the stage and observing the distance required for significant changes in the diffraction pattern that are indicative of sampling a different grain orientation. Fig. 3 shows the diffraction patterns of the reference grain recorded at room temperature (Fig. 3a) and 150°C (Fig. 3b), a temperature which is above the Curie temperature of $BaTiO_3$. Note that Fig. 3a and 3b show orientations of the

neighboring grains as well since the penetration depth of the x-rays were around 20μm as aforementioned. These neighboring grains appear as distinctive spots compared to the reference grain and their orientations were confirmed to be different using an independent orientation fitting. Furthermore, the spots that are identified as originating within the same grain were measured at all positions across the grain and exhibit diffuse scattering between them, indicating that they are not separated by a grain boundary. During the heating cycle from room temperature to above the Curie temperature, the spots gradually converge to one. This is illustrated in an enlarged portion of the diffraction pattern in Fig. 3c. Preceding the phase transformation from tetragonal to cubic, the ferroelectric domains transform to the overall orientation of the grain. At a temperature of 125°C, only one spot can be distinguished in the diffraction pattern. The coalescence of the diffraction spots correlate with the capacitance measurements presented in Fig. 2 and, therefore, the evolution of the ferroelectric domains within the grain. Furthermore, the relative positions of the spots as a function of temperature mimic the changes in the lattice parameters as a function of temperature. These observations suggest that the four different spots correspond to four unique domain orientations in a tetragonal perovskite crystal, a result which will be shown to be consistent with the expected domain wall orientations in this symmetry[26-27].

The changes in the lattice parameters play an important role in the formation of the domains. During cooling, the lattice parameters in the tetragonal structure create an elastic driving force for the formation of the domain variants. Fig. 3(c) shows the temperature evolution of the (215) spots in the heating regime. The close spots are marked with a letter. As the temperature is increased to a value near the Curie temperature, these diffraction spots begin to coalesce. These spots then become the same orientation (identified as E in Fig. 3c) at temperatures above the Curie temperature.

Table 1 shows the orientations of the domains at room temperature and at a temperature above the Curie temperature. The orientations are shown as direction cosines between the crystal lattice and global directions. Each column in the orientation matrices represents the direction cosines of the crystal lattice with respect to the global coordinates. As seen in Table 1, the domain orientations are produced

from the crystals pointing at different global directions. While domains A and D have similar crystal orientations in global coordinates, the orientations of domains B and C can be produced from domain A by rotating approximately 90° around [100] and [010], respectively. The misorientation angles of the respective domain orientations are also reported in Table 1. To obtain the misorientation angles, domain A was selected as the reference domain. The orientations of domains B and C are related to domain A by angles of 89.63° ($\approx 2\tan^{-1}(a/c)$) and 89.41°, respectively. Domain D appears as closely oriented to domain A with a 0.474° misorientation angle. The misorientations of domains B and C were obtained by taking the domain A as reference orientation. By taking into account the varying c/a ratios of the domains (Table 1), the orientations of domain B and C are related with twinning operations as m[011] and m[101] respectively. The orientation relations of the domains are consistent with Keeble's study on the tetragonal single crystal $BaTiO_3$[29].

As the temperature is increased to above the Curie temperature, the diffraction spots coalesce to a single spot, E. The transformation of these spots represents the disappearance of the domain structure within the grain as the Curie temperature is passed and the material becomes paraelectric. From the calculated misorientation angle between the orientations of the domain variants and the orientation of the grain with spot E shown in Table 1, none of the domains have an orientation that precisely equals that of the paraelectric cubic state. Nepochatenko[27] has shown that the domains can rotate a small angle during the cubic-to-tetragonal phase transformation to maintain the strain compatibility as a function of changing lattice aspect ratio. This rotation is relative to the sample coordinate axes and represents a rotation of the entire domain crystal axes; such a rotation is not the same as a polarization rotation involving crystallographic distortions as described in Ref. 30. The rotation angle of the domain with respect to paraelectric phase is referred to as the phase matching angle as described in Ref. 27 and is given by the equation

$$\psi = \cos^{-1}\left(\frac{2+\varepsilon_{11}+\varepsilon_{22}}{\sqrt{2}\sqrt{(1+\varepsilon_{11})^2+(1+\varepsilon_{22})^2}}\right) = \cos^{-1}\left(\frac{a+c}{\sqrt{2}\sqrt{a^2+c^2}}\right) \qquad (2)$$

where ε_{11}, ε_{22} are the spontaneous strain components ($\varepsilon_{11} = (a - a_0)/a_0$, $\varepsilon_{22} = (c - a_0)/a_0$) that represent the lattice parameters for cubic phase (a_0) change to tetragonal (a, c). These angles are required for strain compatibility between the domain and the paraelectric phase[26,27]. The phase matching angle is calculated in the present work to be 0.28°±0.03° from the major axes between the orientation of the ferroelectric domains at room temperature and the high temperature paraelectric cubic state. The comparison of the orientation of the high temperature structure and the ferroelectric domains shows good agreement to the predicted phase matching angle.

The diffraction spots can also be reconciled with the domain structures as follows. When the spontaneous polarization is formed with respect to a paraelectric cubic structure, several different 90° domain wall orientations can form. For instance, for a spontaneous polarization developed parallel to the [001] crystal direction, the domain walls can form parallel to (101), $(\bar{1}01)$, (011) and $(0\bar{1}1)$ planes, creating four domains with perpendicular polarization vectors relative to the [001] polarization direction. These four neighboring domains would have spontaneous polarization vectors parallel to [100], [010], $[\bar{1}00]$ and $[0\bar{1}0]$. In absence of a domain architecture model in which to reconcile the formation of such domains in real space, the domain walls separating $[\bar{1}00]$ and [1 0 0] domains are typically referred to as 180° domain walls as their orientations can be reproduced from one another through a 180° crystallographic rotation. However, the domain architectures in real space can provide more information that is critical to interpreting the μSXRD measurement. A typical "wedge shaped" domain architecture in polycrystalline ferroelectrics is shown in Fig. 4(b)[28]. Ref. 4 discusses that this type of domain architecture exhibits the minimum elastic energy. In Fig. 4(a), the schematic distributions of the domain c-axis orientation variants at room temperature are represented as directions. The structure exhibits four domain variant orientations with c-axes parallel to [001], [100], [010] and $[00\bar{1}]$ relative to the paraelectric reference frame for domains A, B, C, and D, respectively. The

domain walls between domain A and C, C and B, B and D, D and A are (101), (110), (011) and (110) respectively. The angle between the polarization axis of A and C is defined by Eq. (1) and will be equal to a value less than 90°. The angle between C and B is also an angle less than 90° as well as the angle between B and D. Thus, when describing the orientation of domains A, C, B, and D in sequence, the polarization direction of A is not found to be antiparallel to the polarization direction of D. Instead, the two domain orientations are related through an angle that will be referred to as the mismatch angle. The mismatch angle is developed during the cubic-to-tetragonal transformation and can be obtained from the spontaneous strain according to Eq. (1).

For a domain in which polarization is developed parallel to [001], the misorientation between the domain and the paraelectric phase axes can develop on (101), $(\bar{1}01)$, (011) or $(01\bar{1})$ walls which are referred as 90° walls. Considering the paraelectric phase orientation is a reference frame and therefore doesn't change during the cubic-tetragonal phase transformation, two neighboring domains must share a domain wall that is consistent with the orientation of the paraelectric phase. The domain pairs then have domain walls that are perpendicular to each other. For instance, if a domain is separated with the paraelectric phase with (101) domain wall, the neighboring domain must be separated with $(\bar{1}01)$ domain wall with the paraelectric phase in order to have common and stable paraelectric phase that does not change during the phase transformation. Such domains develop a phase matching angle with respect to the paraelectric phase orientation and are misoriented by an angle ($\pm\psi$) as described in Ref. 27.

The mismatch angle between domains A and D in Fig. 4(b) corresponds to twice the phase matching angle between the ferroelectric and paraelectric phase developed during the cubic-to-tetragonal phase transformation. Therefore, in the domain structure example of Fig. 4(b), the ferroelectric polarization direction of domain A is either related to the polarization direction of domain D by a rotation of approximately 180.47° or 0.47° (using values of a = 3.9947 Å and c = 4.0336 Å)[8]. If the two domain orientations A and D are connected in real space, it is electrically unfavorable for them to be related by

a rotation of 0.47°. Therefore, a rotation of 180.47° is more likely. This observation is contrary to common acceptance that domains of opposite polarity are separated by 180° domain walls. While classically defined 180° domain walls may still exist in the present material, they are not measured in the current experiment. Instead, the current experiment provides evidence that unique domain orientations exist in a single grain in which the polarization can be tilted at angles of either 180.47° or 0.47°. These domains may be connected in real space (e.g., as shown for domains A and D in Fig. 4), or they may exist in different regions of the grain. If the domains are connected in real space, the structural nature of the interface between domains of this type is not yet well defined. However, it is noted that the lattice mismatch would require an elastic accommodation mechanism and the increasing lattice aspect ratio with decreasing temperature gradually changes this angle. Possible accommodation mechanisms may include a series of dislocations and/or elastic strain near the domain wall. The region of the diffraction pattern between the diffraction spots shows diffuse scattering (Fig. 3c) which may support either of these mechanisms.

It is also important to mention that 180° domains are sometimes smaller than 1 μm, which is the x-ray beam size used in the present experiment. Considering the x-ray beam penetrates the sample up to 20 μm, the observed diffraction pattern can be considered as describing the domain structure inside the grain, demonstrating that the technique is capable of observing these pseudo-180° domains even though the individual lamella may be thinner than the x-rays beam size.

By considering all the cube faces {100} as a possibility of spontaneous polarizations in tetragonal ferroelectrics, there can be four {110} 90° domain wall types relative to the cubic axis. However, since there are six possible domain variants in tetragonal structures, a total of 24 90° domains wall orientations may develop in a three dimensional arrangement. Due to the ambiguity of the directions in X-rays where the positive and negative directions are not detectable, a maximum of 12 domain wall types could be detected using this μSXRD technique.

The orientations demonstrate that the spontaneous polarization vectors of the domains form perpendicular to the cube faces, {100}, or parallel to the cube edges, <100>. To illustrate this further, Fig. 5 shows the 001 pole figure for the domains inside of the reference grain at room temperature (Fig. 5a) and the 100 pole figure for the reference grain orientation in the high temperature cubic phase (Fig. 5b). There is correlation between the [001] of the low temperature orientations and the <001> of the high temperature orientations.

A closer inspection of the diffraction patterns as a function of distance along the sample surface in 1.5 μm steps demonstrates that the spots representing different orientations have varying intensities. Because the thickness of the domains is smaller than the beam size (1 μm), different domains are illuminated by the beam at different sample positions. Since the same domain diffraction patterns are observed as the sample stage is moved, this three-dimensional arrangement of the domain variants likely repeats itself inside the grain.

During heating from room temperature, the domains experience a slight orientation rotation and lattice parameter changes that result in the individual diffraction spots converging into a single diffraction spot at the Curie temperature. Fig. 6(a) shows the evolution of the a/c ratio calculated as a function of temperature. The error bars were determined from independent a/c calculations of the domains at given temperature. During the phase transformation, the relative change in orientations of the domains can be calculated from the refinement of the peak position. These orientation relationships are related directly to the changes in the lattice parameter. For instance, the angles between domains A and C and between domains B and D have been calculated to be 89.61° and 89.58°, respectively, at a temperature of 90°C. The angles between these domain pairs were calculated for all the different temperature from the (251) and (351) diffraction peaks. Fig. 6(b) shows the angular separations between the domain pairs A and C as well as B and D during heating. As the sample is heated to temperatures approaching the Curie temperature, the ferroelectric domains become more closely oriented to one another as well as become more closely oriented to the high temperature cubic orientation. The domains converge to a single orientation at temperatures near and above the Curie

temperature. The angular separation between the domains correlates well with the misorientation angle that is calculated from the c/a ratio using Eq. (1). The angular separation of the domain pairs is also well correlated with the capacitance versus temperature measurements as shown in Fig. 2.

IV. CONCLUSIONS

The evolution of the ferroelectric domain structure inside the polycrystalline $BaTiO_3$ was investigated during quasistatic heating using scanning X-ray microdiffraction (μSXRD). Four domains are observed for certain reflections and the polarization direction associated with two of these domains are related by an angle of either 180.47° or 0.47°. These domains are classically defined as 180° domains but are clearly separated in the diffraction experiment. The crystallographic relationships of the domains are explained using a domain structure model by Nepochatenko. While heating the polycrystalline $BaTiO_3$ from room temperature to above the Curie temperature, the ferroelectric domains coalesce by slight orientation rotations relative to the paraelectric axes that reflect their changing lattice aspect ratio. With the direct experimental observations, the technique is shown to be capable of studying ferroelectric domain structure embedded in polycrystalline ferroelectrics.

ACKNOWLEDGEMENTS

This project is funded by the APS which is supported by the US-DOE under contract no. W-31-109-ENG-38. The Advanced Light Source is supported by the Director, Office of Science, Office of Basic Energy Sciences, Materials Sciences Division, of the U.S. Department of Energy under Contract No. DE-AC02-05CH11231 at Lawrence Berkeley National Laboratory and University of California, Berkeley, California. One of the authors (JLJ) acknowledges support from the National Science Foundation under award DMR-0746902. The authors would like to thank Dr. Ulrich Lienert (APS) for helpful discussions and Seung-Yub Lee (ISU), Guillaume Geandier (ALS) and Sirine Fakra (ALS) for help in the experiments.

Figure Captions

Fig. 1. SEM micrograph of the $BaTiO_3$ sample investigated in this study.

Fig. 2. Capacitance change in BaTiO3 as a function of temperature. The estimated uncertainties to determine the capacitance and temperature are ±0.1 nF and ±0.5°C respectively.

Fig. 3. Laue diffraction patterns of $BaTiO_3$ recorded at (a) room temperature, (b) above Curie temperature (150°C). (c) The evolution of (215) spots of ferroelectric domains in $BaTiO_3$

Fig. 4. (a) The schematic distributions of the domain variants in misorientation axes. The misorientation axes were based on the cubic grain and the angles were exaggerated for clarity. (b) The three dimensional arrangement of the domains.

FIG. 5. (a) 001 pole figure of the ferroelectric domain orientations at room temperature. (b) 100 pole figure of the grain at a temperature above the Curie temperature. For each plot, the specified crystal directions were drawn in global directions where the origin of the plot shows the surface normal. Wulff net is overlaid for clarity. The orientations correspond to those presented in Table 1. The orientations at both temperatures have almost identical orientations and show a direct correlation between cubic and tetragonal phase.

Fig. 6. (a) The evolution of a/c ratio as a function temperature. (b) The angles between domain pairs (A/C and B/D) as a function of the temperature. Black curves were calculated by using tangent formula (Eq. 1). The estimated uncertainties to determine the orientation angle and temperature are ±0.05° and ±0.5°C respectively.

Table Captions

Table 1. The orientations and misorientations of the domains seen at room temperature and above Curie temperature. The misorientations between the domains were calculated by selecting either domain A or domain E as the reference domain.

[1] F. Jona, G. Shirane, *Ferroelectric crystals*, (Oxford: Pergamon Press, 1962).
[2] B. Jaffe, *Piezoelectric ceramics*, (Academic Press, London, 1971).
[3] G. H. Haertling, Journal of the American Ceramic Society, **82**, 4 (1999).
[4] G. Arlt, Journal of Materials Science, **25** (1990).
[5] F. X. Li, D. N. Fang, A. K. Soh, Scripta Materialia **54** (2006).
[6] J. Harada, T. Pedersen, Z. Barnea, **A26**, 336 (1970).
[7] T. L. Jordan, Z. Ounaies, *Piezoelectric ceramics characterization*, NASA Technical Reports, Langley Research Center (2001).
[8] R. C. Rogan, N. Tamura, G. A. Swift, E. Ustundag, Nature Materials, Volume 2 (2003).
[9] X. Tan, J. K. Shang, Journal of Applied Physics, **96**, 5 (2004).
[10] K. A. Schönau, M. Knapp, H. Kungl, M. J. Hoffmann, H. Fuess, Physical Review B, **76**, 14 (2007).
[11] X. R. Huang, S. S. Jiang, W. J. Liu, X. S. Wu, D. Feng, Z. G. Wang, V. Han, J. Y. Wang, J. Appl. Cryst. **29**, 371 (1996).
[12] F. Ernst, M. L. Mulvihill, O. Kienzle, M. Ruhle, J. Am. Ceram. Soc., **84,** 8, 1885 (2001).
[13] S. Balakumar, J. B. Xu, J. X. Ma, S. Ganesamoorthy, I. H. Wilson, Jpn. J. Appl. Phys., **36**, 5566, (1997).
[14] S. V. Kalinin, D. A. Bonnell, Appl. Phys. Lett. **78**, 1116 (2001).
[15] J-H Chen, B-H Hwang, T-C Hsu, H-Y Lu, Materials Chemistry and Physics **91**, 67 (2005).
[16] W. Chang, A. H. King, K. J. Bowman, Journal of Materials Research, **22**, 2845 (2007).
[17] M. E. Lines, A. M. Glass, "*Principles and applications of ferroelectrics and related materials*", (Oxford, Clarendon Press, 1977).
[18] P. Goudeau, N. Tamura, R. Spolenak, H. A. Padmore, Materials Science Forum, **490-491**, 672 (2005).
[19] J-S Chung, G. E. Ice, Journal of Applied Physics, **86**, 9, 5249 (1999).
[20] N. Tamura, A. A. MacDowell, R. Spolenak, B. C. Valek, J. C. Bravman, W. L. Brown, R. S. Celestre, H. A. Padmore, B. W. Batterman, J. R. Patel, Journal of Synchrotron Radiation, **10**, 137 (2003).
[21] T. A. Bryne, D. P. Cann, J. Am. Ceram Soc., **87**, 5, 875 (2004).
[22] F. C. Frank, Metallurgical Transactions A, **19A**, 403 (1988).
[23] A. Morawiec, Acta Cryst., **A53**, 273 (1997).
[24] S. Sundararaghavan, N. Zabaras, Acta Materialia, **55**, 1573 (2007).
[25] P. Dawson, D. Boyce et al., "The DPLAB Polycrystal Library at Cornell", http://anisotropy.mae.cornell.edu
[26] J. Sapriel, Physical Review B, **12**, 11, 5128 (1975).
[27] V. A. Nepochatenko, Ferroelectrics, **341**, 1, 97-102 (2006).
[28] W. J. Merz, Phys. Rev., **88**, 421 (1952).
[29] D. S. Keeble, A. T. Thomas, Journal of Applied Crystallography, **42**, 480 (2009).
[30] M. Ahart, M. Somayazulu, R. E. Cohen, P. Ganesh, P. Dera, H-K. Mao, J. H. Russell, R. J. Hemley, Y. Ren, P. Liermann, Z. Wu, Nature**, 451**, 545 (2008).

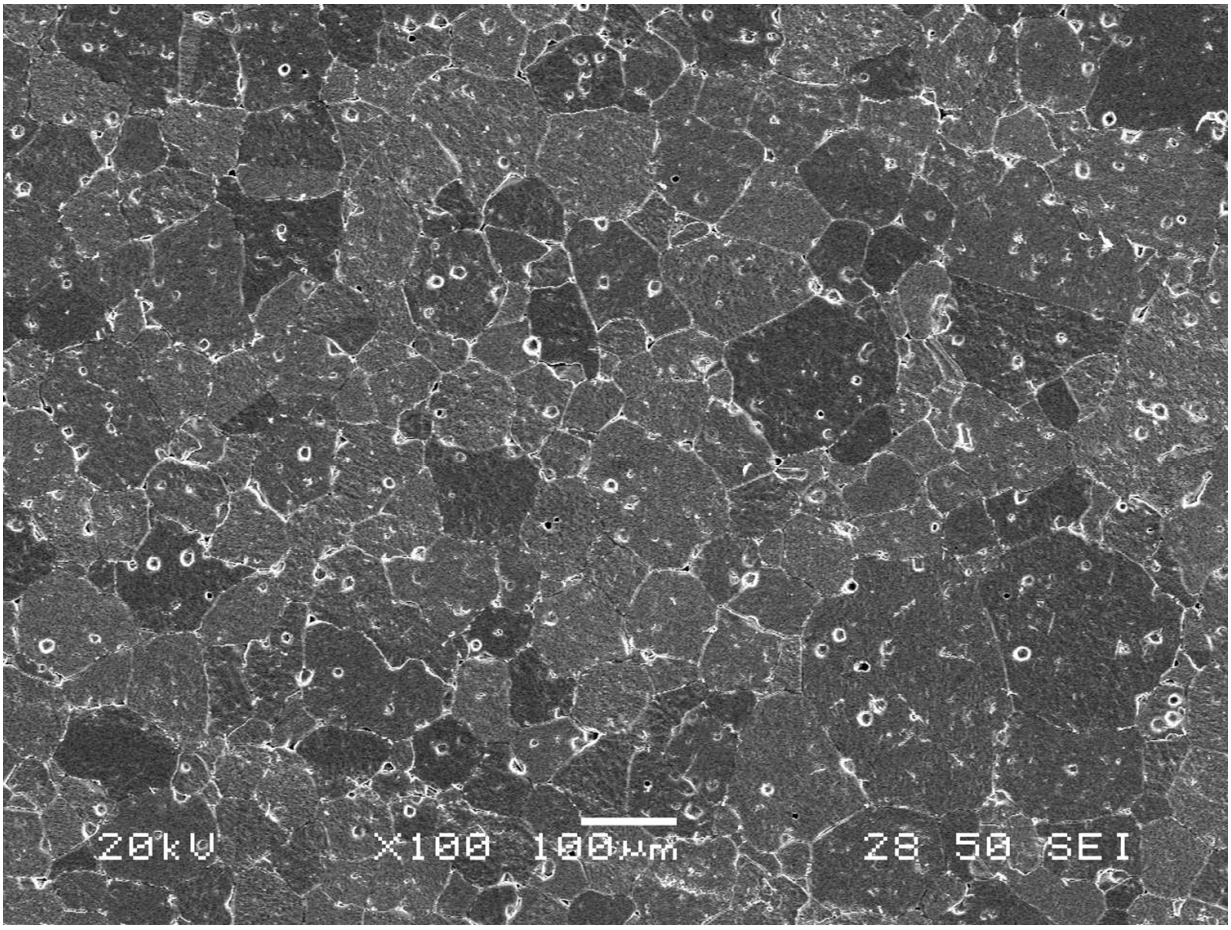

Figure 1

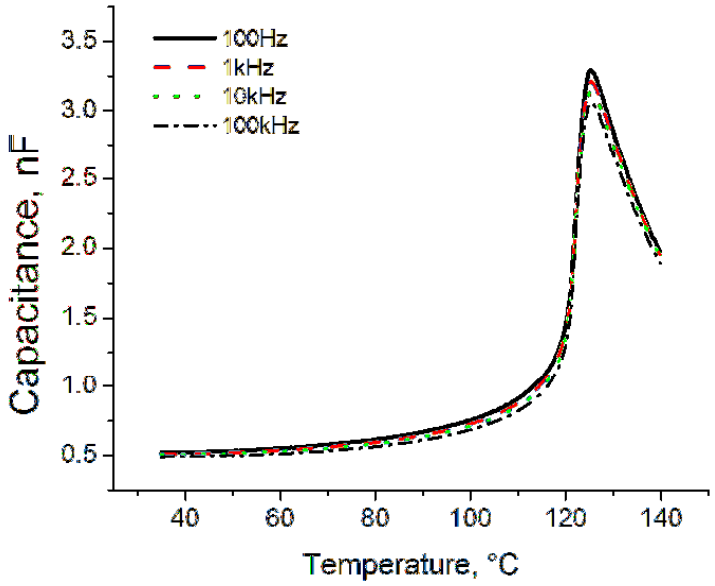

Figure 2

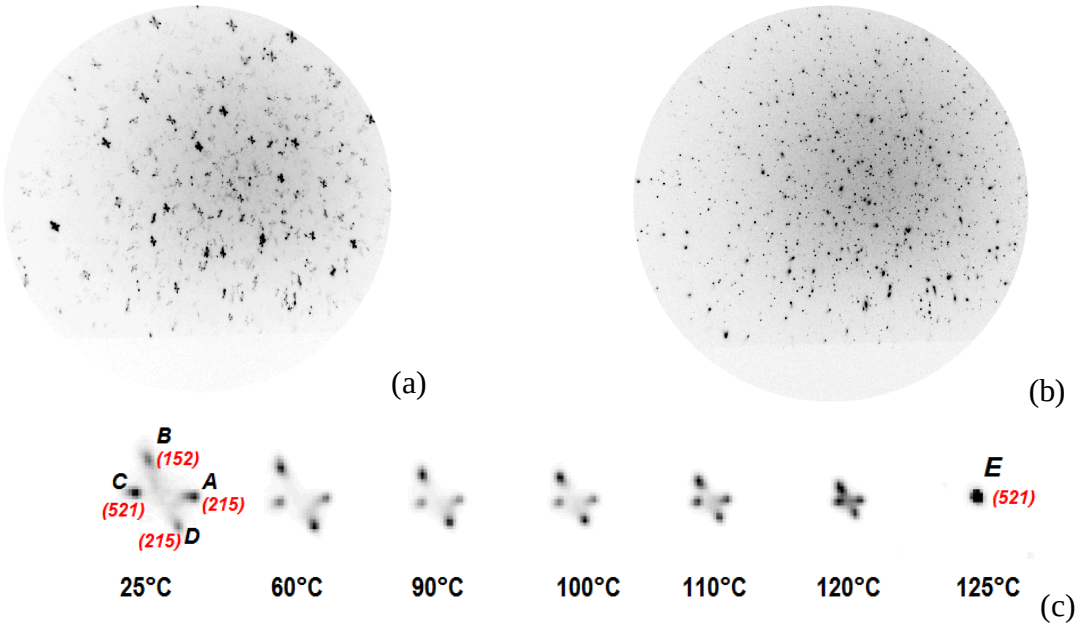

Figure 3

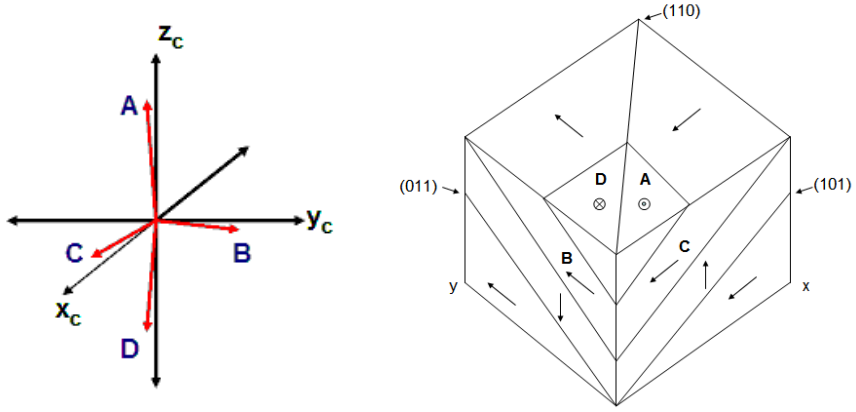

(a) (b)

Figure 4

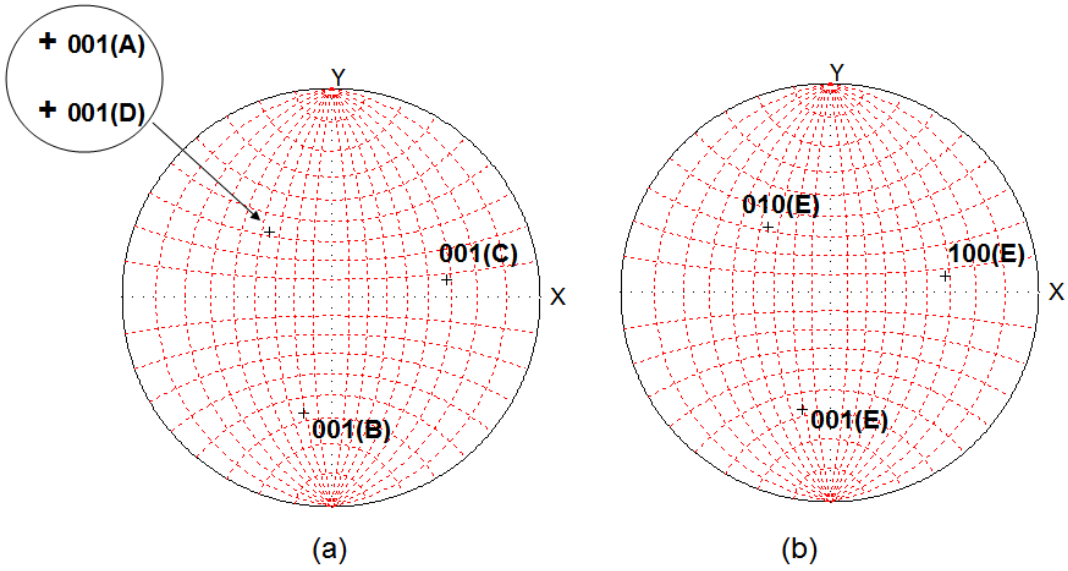

(a) (b)

Figure 5

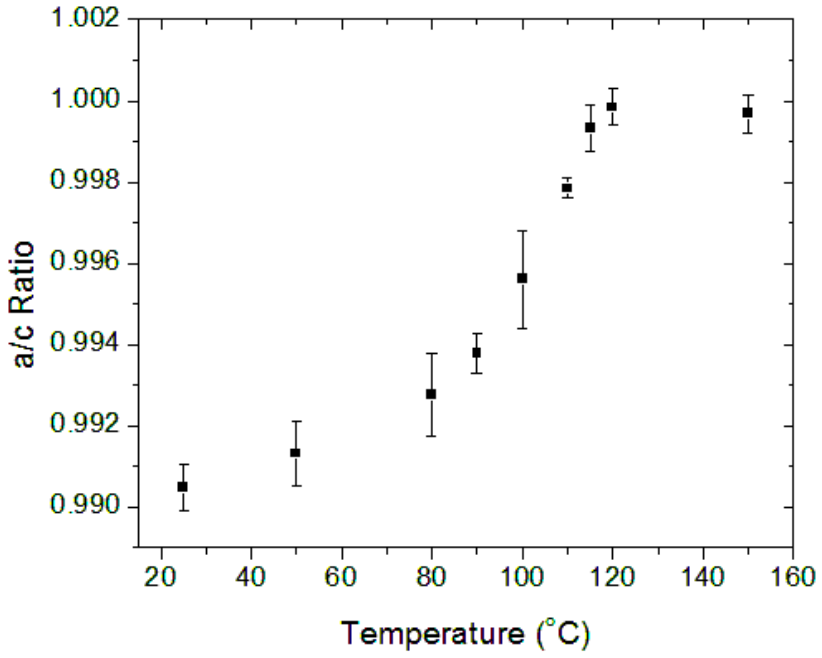

Figure 6(a)

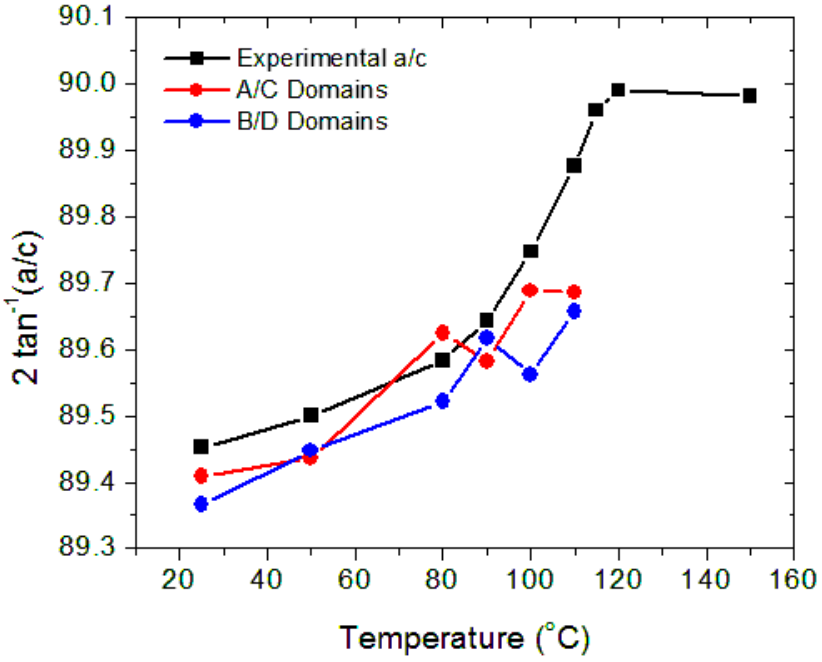

Figure 6(b)

Domain		Orientation Matrix	Misorientation Angle, [Axis]	Misorientation Angle, [Axis]	c/a Ratio
Room Temperature	A	0.846 0.193 -0.497 0.119 0.8340 0.529 0.519 -0.507 0.687	Reference	0.36°, [-0.23 0.6 0.77]	1.01
	B	0.842 -0.500 -0.200 0.118 0.534 -0.8367 0.526 0.681 0.509	89.63°, [1 0 0]	89.47°, [1 0 0]	1.088
	C	0.507 0.192 0.840 -0.527 0.839 0.126 -0.681 -0.508 0.527	89.41°, [0 1 0]	89.67°, [0 1 0]	1.011
	D	0.842 0.194 -0.502 0.119 0.843 0.525 0.525 -0.502 0.687	0.47°, [0.59 -0.66 -0.47]	0.2°, [0.9 -0.41 0.18]	1.098
$T > T_C$ (150° C)	E	0.842 0.194 -0.502 0.119 0.841 0.526 0.524 -0.504 0.686	n/a	Reference	1

Table 1